# Rapid Measurement of Bulk Flow Propagators

Noah Stocek

April, 2018

# Acknowledgements

This project would not have been possible without the help of Dr. Ben Newling, Amy-Rae Gauthier, and Alex Adair.

# Table of Contents

# List of Figures

# Abstract

Bipolar NMR gradients are known to be able to motion encode the velocity of spins of a flowing sample. Using these gradients, we can measure the displacement of these spins and find the probability of each displacement value, which has a maximum at the modal spin displacement value. The probabilities of these displacements are known as the propagator. Using the time between excitation and measurement we can then turn these displacements into velocities.

The UNB MRI Centre's 2.4 tesla magnet is ideally suited to measure these propagators. Here, it is used to apply bipolar gradients at increasing values of motion encoding gradient in an effort to sample Fourier conjugate of the displacement space as efficiently as possible. We measured these propagators without any spatial encoding, to construct the bulk flow propagator.

# Chapter 1

# Magnetic Resonance Basics

## 1.1 Quantum Mechanical Picture

When dealing with atomic nuclei, one must begin from quantum mechanics. These nuclei are the topic of Nuclear Magnetic Resonance (NMR), so it is in quantum mechanics that a discussion on NMR should begin. While NMR deals with large numbers of spins, so much so that this collection of spins will act as a continuous system, and display what we call ensemble properties, it is still at its core quantum mechanical. For nuclei with spin $\frac{1}{2}$, we find that the only magnetic moment is that of a dipole, while integer spin leads to both a dipole moment and a quadrupole moment. In NMR, a nucleus with net spin (and its dipole moment) is placed in a uniform magnetic field, $B_0$ pointing in what we define as the $z$-direction (longitudinal).

We find from Schrödinger's equation that a system evolving under a

Hamiltonian, $\hat{\mathcal{H}}$, that is constant in time (such as that imposed by our magnetic field) has the time evolution

$$|\Psi(t)\rangle = e^{\frac{-i\hat{\mathcal{H}}t}{\hbar}}|\Psi(0)\rangle \tag{1.1}$$

The appropriate Hamiltonian for our dipole in a magnetic field is the Zeeman Hamiltonian, which has the form

$$\hat{\mathcal{H}}_{Zeeman} = -\boldsymbol{\mu} \cdot \boldsymbol{B_0} \tag{1.2}$$

The magnetic dipole moment of a spin $\frac{1}{2}$ nucleus is $\boldsymbol{\mu} = \gamma\hbar I_z\hat{\boldsymbol{z}}$ [1] where $I_z$ is the component of the spin along the $z$-axis and $\gamma$ is the gyromagnetic ratio of the nucleus, which plays a central role in NMR. Given this form of the dipole moment, our Zeeman Hamiltonian of equation (1.2) becomes

$$\hat{\mathcal{H}} = -\gamma\hbar I_z B_0 \tag{1.3}$$

For this Hamiltonian, the time evolution operator of this spin system is

$$e^{i\gamma B_0 I_z t} \tag{1.4}$$

Which is the form of a clockwise, time dependant rotation operator, rotating at what is called the Larmor frequency: $\omega_0 \equiv \gamma B_0$. For typical values of $B_0$, this lies in the radio frequency (RF) range. The energy separation between spin states in a magnetic field is thus $\gamma\hbar B_0$ since $I_z$ increments in

integers. As we make the bridge from this quantum mechanical picture to that of a more useful semi-classical approach, the fact that this energy separation is so small ( $7 \times 10^{-8}$ eV for Hydrogen in a 2.4 tesla magnetic field) will be instrumental.

## 1.2 Nuclear Paramagnetization

Paramagnetization is the phenomenon whereby a material gains its own temporary magnetization when placed in an external magnetic field, in the direction of this field. In NMR, spin paramagnetization is observed and helps us make the bridge from a quantum mechanical approach to a semi-classical one in which we can consider ensemble behaviour.

For a spin $\frac{1}{2}$ system in a uniform magnetic field, there are 2 possible energy values given by the Zeeman Hamiltonian: $\pm\frac{1}{2}\gamma\hbar B_0$. If we assume that the sample has reached thermal equilibrium in the magnetic field, and that our sample contains a large number of nuclei, then the population of each energy level is governed by the Boltzmann Law of statistical mechanics [2]

$$P(E_{I_z}) = P_{I_z} \propto e^{\frac{\gamma\hbar I_z B_0}{\tau}} \tag{1.5}$$

where $\tau = k_B T$ with $k_B$ being the Boltzmann constant and $I_z$ being $\pm\frac{1}{2}$ for a spin $\frac{1}{2}$ nucleus. We use Boltzmann statistics here since the sample is assumed to be at a high temperature, compared to our energy separation.

For a sample containing $N$ spins, there is a net magnetization vector of

$$\boldsymbol{M} = M_x\hat{\boldsymbol{x}} + M_y\hat{\boldsymbol{y}} + M_z\hat{\boldsymbol{z}} \tag{1.6}$$

Since in this system there is no preferred direction in the $xy$ plane (transverse), $M_x$ and $M_y$ are both zero since contributions from individual nuclei cancel each other out, and only $M_z$ is non-zero. This $z$ component is

$$M_z = N\langle\mu_z\rangle = N\gamma\hbar\frac{\sum_{I_z} I_z P_{I_z}}{\sum_{I_z} P_{I_z}} = \frac{N\gamma\hbar}{2}\left[\frac{e^{\frac{\gamma\hbar B_0}{2\tau}} - e^{\frac{-\gamma\hbar B_0}{2\tau}}}{e^{\frac{\gamma\hbar B_0}{2\tau}} + e^{\frac{-\gamma\hbar B_0}{2\tau}}}\right] \tag{1.7}$$

Now, since $\gamma\hbar B_0 \ll \tau$ for all reasonable values of magnetic fields and temperature, this sample is always in the high temperature regime. Because of this, we can make a high temperature approximation, and truncate a Taylor expansion of the exponentials in equation (1.7)

$$e^{\pm\frac{\gamma\hbar B_0}{2\tau}} \approx 1 \pm \frac{\gamma\hbar B_0}{2\tau} \tag{1.8}$$

We can substitute this into equation (1.7) and get

$$M_{z(0)} = \frac{N\gamma^2\hbar^2}{4}B_0 \tag{1.9}$$

By employing this statistical description of the sample, the discussion has become classical [3], and will remain so for the remainder of this thesis.

## 1.3 Resonant Excitation

For our sample of consideration, the macroscopic angular momentum vector of our spin ensemble is given by $\boldsymbol{L} = \frac{1}{\gamma}\boldsymbol{M}$. The torque acting on a dipole moment in a magnetic field is given by $\boldsymbol{\tau} = \boldsymbol{\mu} \times \boldsymbol{B}$ [4]. By equating the rate of change of the angular momentum and the torque, we find

$$\frac{d\boldsymbol{M}}{dt} = \gamma \boldsymbol{M} \times \boldsymbol{B} \tag{1.10}$$

For $\boldsymbol{B} = B_0\hat{\boldsymbol{z}}$ and $\boldsymbol{M} = M_z\hat{\boldsymbol{z}}$ there is clearly no torque. However, if an oscillating magnetic field, say

$$\boldsymbol{B_1} = B_1 \cos(\omega_0 t)\hat{\boldsymbol{x}} - B_1 \sin(\omega_0 t)\hat{\boldsymbol{y}} \tag{1.11}$$

is applied, where $\omega_0$ is the Larmor frequency from before, then equation (1.10) becomes

$$\begin{aligned} \frac{dM_x}{dt} &= \gamma[M_y B_0 + M_z B_1 \sin(\omega_0 t)] \\ \frac{dM_y}{dt} &= \gamma[M_z B_1 \cos(\omega_0 t) - M_x B_0] \\ \frac{dM_z}{dt} &= \gamma[-M_x B_1 \sin(\omega_0 t) - M_y B_1 \cos(\omega_0 t)] \end{aligned} \tag{1.12}$$

Given the initial condition of $\boldsymbol{M}(0) = M_0\hat{\boldsymbol{z}}$, the solutions to equations (1.12) are

$$
\begin{aligned}
M_x &= M_0 \sin(\omega_1 t) \sin(\omega_0 t) \\
M_y &= M_0 \sin(\omega_1 t) \cos(\omega_0 t) \\
M_z &= M_0 \cos(\omega_1 t)
\end{aligned}
\tag{1.13}
$$

Where $\omega_1 \equiv \gamma B_1$, and for a given time, we define the tip angle $\alpha \equiv \omega_1 t$. From equations (1.13) we can see that this tip angle determines the angle that the magnetization vector is tipped into the transverse plane.

## 1.4 Relaxation and the Free Induction Decay

The RF pulse served the purpose of disturbing the spin system from the equilibrium state described by $\boldsymbol{M} = M_0 \hat{\boldsymbol{z}}$. As soon as this equilibrium is disturbed, the magnetization vector begins restoring to this equilibrium state via energy exchange with the surrounding reservoir (lattice). The restoration of the $z$ component back to equilibrium is governed by

$$
\frac{dM_z}{dt} = -\frac{M_z - M_0}{T_1} \tag{1.14}
$$

Where $T_1$ is called the longitudinal (spin-lattice) relaxation time constant. If, at time t=0 (measured from when $B_1$ is turned off), the remaining longitudinal magnetization is $M_z(0)$, then the solution of equation (1.14) is

$$M_z(t) = M_z(0)e^{-\frac{t}{T_1}} + M_0(1 - e^{-\frac{t}{T_1}}) \tag{1.15}$$

There is also a mechanism by which the transverse magnetization vector decays. This is called transverse (spin-spin) relaxation. This is when the spins approach thermal equilibrium by exchanging energy with each other, and it occurs at a rate equal to or lesser than longitudinal relaxation. This spin-spin behaviour is governed by

$$\frac{dM_{x,y}}{dt} = -\frac{M_{x,y}}{T_2} \tag{1.16}$$

Where $M_{x,y}$ is the magnitude of the transverse magnetization and $T_2$ is the spin-spin relaxation time constant. If at time t=0 the excited transverse magnetization is $M_{x,y}(0)$, the solution to equation (1.16) is

$$M_{x,y}(t) = M_{x,y}(0)e^{-\frac{t}{T_2}} \tag{1.17}$$

The most basic NMR experiment that one can employ is the Free Induction Decay (FID). In this experiment we consider a sample at thermal equilibrium in a homogeneous magnetic field, $\boldsymbol{B} = B_0\hat{\boldsymbol{z}}$ with an equilibrium magnetization vector $\boldsymbol{M} = M_0\hat{\boldsymbol{z}}$. If the RF pulse is applied for a period of time such that $\alpha = \frac{\pi}{2}$, then the magnetization vector is tipped entirely into the transverse plane. The spins will quickly come into thermal equilibrium with each other and the net transverse magnetization vector will decay away. From equations (1.13) and (1.17), we know that the time evolution of this

magnetization vector is as follows

$$\boldsymbol{M}(t) = [M_0 \cos(\omega_0 t)\hat{\boldsymbol{x}} + M_0 \sin(\omega_0 t)\hat{\boldsymbol{y}}]e^{-\frac{t}{T_2}} \tag{1.18}$$

Here, we can define $M_+ = M_x + iM_y$ to simplify this

$$M_+ = M_0 e^{i\omega_0 t} e^{-\frac{t}{T_2}} \tag{1.19}$$

This tells us that there are two parts to the magnetization vector, a term that oscillates around $B_0$ at the Larmour frequency and a decay term that is governed by $T_2$. This can be seen very clearly in the ideal FID data set shown in Figure 1.1, where there is an oscillation, in a decay envelope (described by $T_2$).

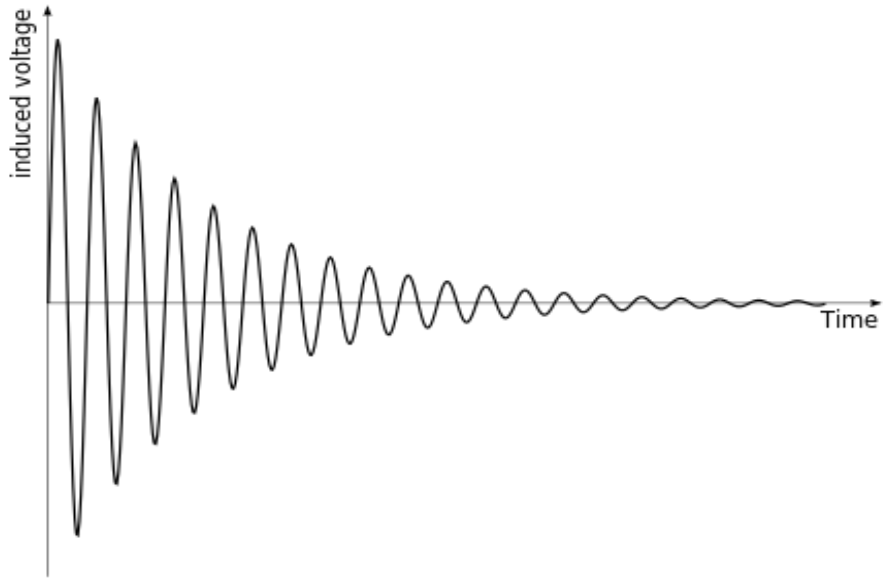


Figure 1.1: Ideal FID data. Courtesy of www.wikipedia.org.

# Chapter 2

# Motion Encoding

## 2.1 Magnetic Field Gradients

The expression for the Larmor frequency from before can be completely generalized as

$$\omega_0 = \gamma |\boldsymbol{B}_{tot}| \tag{2.1}$$

This general expression now allows us to accommodate magnetic field gradients, that is, magnetic fields whose magnitude depend on position. Given a gradient in the $z$-component of the magnetic field, $\boldsymbol{G} = \nabla B_z$, equation (2.1) becomes spatially dependent and has the form

$$\omega_0(\boldsymbol{r}) = \gamma(B_0 + \boldsymbol{r} \cdot \boldsymbol{G}) \tag{2.2}$$

The fact that the spins now precess about the $z$-direction at a spatially dependent rate is of incredible use in Nuclear Magnetic Resonance. It can be used to spatially resolve structures in samples (Magnetic Resonance Imaging or MRI), to obtain information about the translation of molecules, or both.

Consider again the transverse magnetization , $M_+ \equiv M_x + iM_y$. For the moment, we will disregard relaxation as this can be added in very easily afterwards. This is now spatially dependent as well, $M_+ = M_+(\boldsymbol{r}, t)$. Employing equation (2.2), the time evolution of this magnetization in the co-rotating frame, in terms of its initial value is [5]

$$M_+(\boldsymbol{r}, t) = M_+(\boldsymbol{r}, 0)e^{i\gamma t(\boldsymbol{r}\cdot\boldsymbol{G})} \tag{2.3}$$

The spatially dependent oscillatory term in equation (2.3) makes it very clear that the phase of this magnetization evolves according to its position. This phase evolution is shown in Figure (2.1), where the top line depicts a pulse that tips the magnetization fully into the transverse plane, followed by a constant gradient pulse which creates a spatially dependent phase.

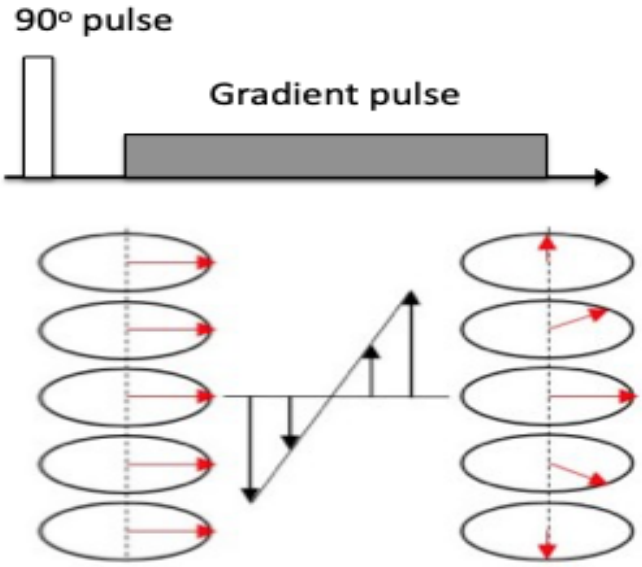


Figure 2.1: Evolution of MR signal phase in magnetic field gradient. Modified from www.magritek.com.

Each circle in this figure represents an isochromat, which is a group of spins which all resonate at the same frequency in a magnetic field gradient. As the phase on these isochromats evolves, a helix of polarization develops in space. Under a certain gradient of value $G\hat{\boldsymbol{z}}$, applied for a time $T_p$, this helix has a wavelength of

$$\boldsymbol{\lambda} = \frac{2\pi}{\gamma G T_p}\hat{\boldsymbol{z}} \tag{2.4}$$

Where we can see that the wavelength gets shorter the longer that the gradient is applied. It is natural to now define a reciprocal space (k-space), by

$$\boldsymbol{k} \equiv \frac{2\pi}{|\boldsymbol{\lambda}|}\hat{\boldsymbol{\lambda}} = \gamma G T_p \hat{\boldsymbol{z}} \tag{2.5}$$

The evolution of magnetization in equation (2.3) can now more compactly be written as

$$M_+(\boldsymbol{r}, t) = M_+(\boldsymbol{r}, 0) e^{i(\boldsymbol{k}\cdot\boldsymbol{r})} \tag{2.6}$$

If the spin density is determined by normalizing this magnetization by the total, initial sample magnetization, $\rho(\boldsymbol{r}) = M_+(\boldsymbol{r}, 0)/M_+(0)$, then by integrating to get the total signal, we find that the signal obtained is the Fourier Transform of this spin density. In an imaging experiment, as many of these $\boldsymbol{k}$-space points are obtained as are desired, and are then reconstructed to obtain an image.

## 2.2 Bipolar Gradients

The reciprocal space defined above is useful for imaging, as it contains information on the static position, $\boldsymbol{r}$ of spin isochromats. However, for motion encoding we wish to obtain information about the dynamic displacement, $\boldsymbol{R}$, of isochromats. For this, we must employ bipolar gradients.

A bipolar gradient has a gradient of strength $g$ ($g$ is traditionally used to denote a motion encoding gradient, while $G$ for imaging gradient) applied for $\frac{T_p}{2}$, followed by a gradient of -$g$ applied for $\frac{T_p}{2}$. A schematic for this type

of gradient can be seen in Figure (2.2). If the isochromats remain stationary, then the second gradient pulse simply restores all of the isochromats to their original states, and no phase accumulates.

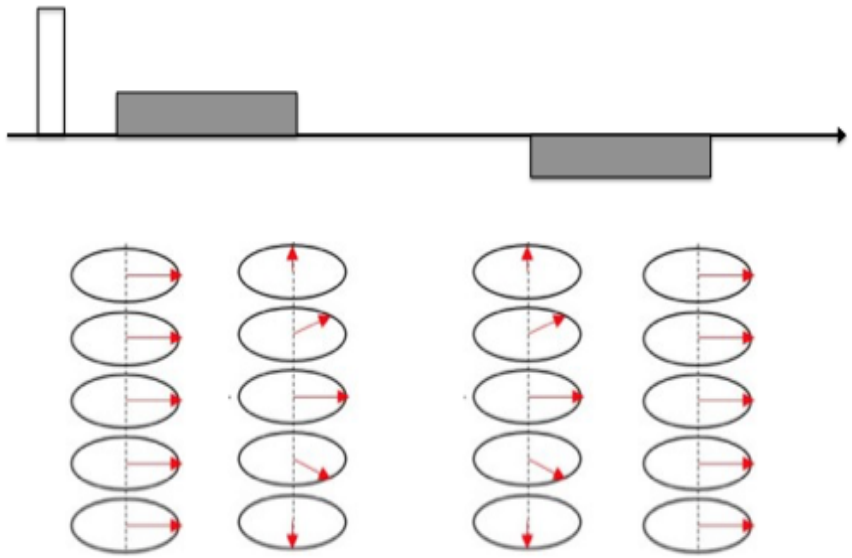

Figure 2.2: Evolution of phase in bipolar magnetic field gradient. Modified from www.magritek.com.

If, however, there is molecular translation between $t$=0 when the RF pulse is applied and $t = T_p$ when data are acquired, then a net phase is accumulated. For a nucleus with a time dependent position, $\boldsymbol{r} = \boldsymbol{r}(t)$, then the accumulated phase is

$$\phi(t) = \gamma \int_0^t \boldsymbol{g}(t') \cdot \boldsymbol{r}(t') dt' \tag{2.7}$$

To examine this phase, we can Taylor expand the position

$$\boldsymbol{r}(t) = \boldsymbol{r}_0 + \boldsymbol{v}t + \frac{1}{2}\boldsymbol{a}t^2 + \dots \tag{2.8}$$

From this expansion, we find the phase to be

$$\phi(t) = \gamma \left( r_0 \int_0^t g(t')dt' + v \int_0^t g(t')t'dt' + \dots \right) \tag{2.9}$$

For a bipolar gradient, $\int_0^t g(t')dt' = 0$, and assuming constant velocity no higher order terms exist, so the accumulated phase is

$$\phi(t) = \gamma v \int_0^t g(t')t'dt' \tag{2.10}$$

For a symmetric gradient, our expression for reciprocal coordinate yields $k = 0$ (here it is said that one is making measurements at the centre of k-space). We can define a new reciprocal space, conjugate to the displacement, $\boldsymbol{R}$, which is called $\boldsymbol{q}$. The concept of $q$-space was introduced by Paul Callaghan [5]. Given a bipolar gradient of amplitude g and duration $T_p$ (in total), the expression for our $q$-space coordinate is

$$\boldsymbol{q} = \gamma g \frac{T_p}{2} \hat{\boldsymbol{z}} \tag{2.11}$$

## 2.3 Bulk Flow Propagators

A propagator is a quantity which contains information on the probability that a molecule in a sample is displaced by $\boldsymbol{R} = \boldsymbol{r}_2 - \boldsymbol{r}_1$ over the time $\frac{T_p}{2}$

[6]. Specifically, a bulk flow propagator contains this information for the entire sample with no spatial encoding. In analogy with imaging, this can be done by sampling as many points in $q$-space as possible, and reconstructing the probability of the corresponding displacement values. If we denote the displacement probability by $P(\boldsymbol{R}, T_p)$, then the signal obtained at time $T_p$ is

$$S(\boldsymbol{q}, T_p) = \int P(\boldsymbol{R}, T_p) e^{i(\boldsymbol{q}\cdot\boldsymbol{R})} d\boldsymbol{R} \tag{2.12}$$

If motion encoding is done strictly in the $z$-direction (i.e. $\boldsymbol{g} = g\hat{\boldsymbol{z}}$) then equation (2.12) reduces to a 1-dimensional Fourier Transform

$$S(q, T_p) = \int P(R_z, T_p) e^{iqR_z} dR_z \tag{2.13}$$

The propagator is thus the inverse Fourier Transform of the signal obtained.

The goal, then, in measuring a bulk flow propagator is to sample as many points in $q$-space as possible. This can be done by applying a string of bipolar gradients, exciting before gradient application and acquiring after each one. To acquire different $q$-space points, the successive gradients must increment either in magnitude or duration (this can be seen by inspection of equation (2.11)). Since our propagator is a measure of the average motion of the fluid over the time $T_p$, and our flow is, in reality, somewhat complex, some fluid elements may speed up or slow down. If $T_p$ is different for each $q$-space point, when the propagator is reconstructed it will have information

about motion averages over different lengths of time and will therefore be somewhat distorted, so the wise decision is to increment gradient magnitude. An example of a pulse sequence that varies g is shown in Figure (2.3). A pulse sequence, such as that shown, shows the application of RF pulses and gradients in a chronological order. In this sequence, the recycle time $T_R$ is the length of time between successive RF pulses, and must larger than or equal to $T_p$. While this is one possible sequence, more will be discussed later.

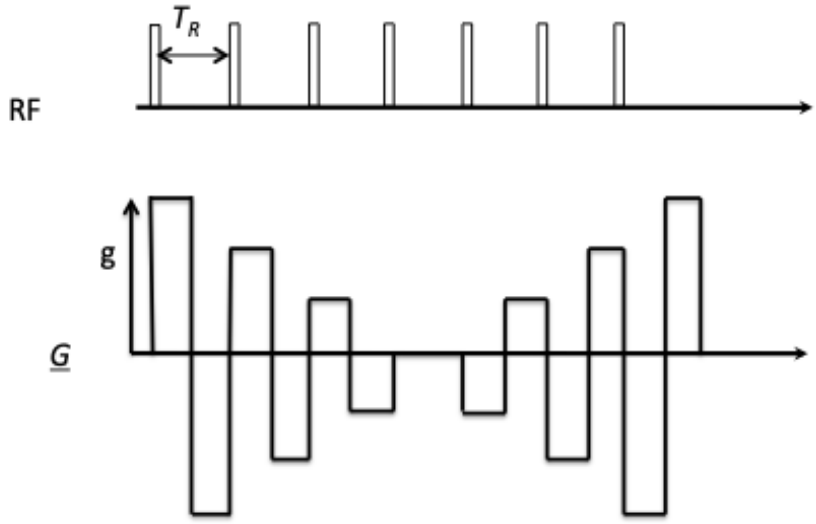


Figure 2.3: Example of a pulse sequence that measures a bulk flow propagator

### 2.3.1 Field of Flow

An important parameter to consider in the measurement of a propagator is the field of flow. If, between each bipolar gradient, the magnitude is incremented by an amount $\Delta g$, then we are incrementing through $q$-space by

an amount

$$\Delta q = \gamma \Delta g \frac{T_p}{2} \tag{2.14}$$

This is the difference between consecutively acquired $q$-space points. This difference is important in determining the sensitivity of the propagator to different velocities, which is governed by a parameter called field of flow, calculated as

$$FoF \equiv \frac{1}{\Delta q} = \frac{1}{\gamma \Delta g \frac{T_p}{2}} \tag{2.15}$$

We can see from this that larger gradient values and/or longer acquisition times lead to increased range of velocities that are measurable. This field of flow is, in actuality, a measure of maximum measurable displacement, in order to determine velocity, we must divide this by $\frac{T_p}{2}$, and thus our range of measurable velocities is

$$v_{max} = \frac{FoF}{\frac{T_p}{2}} = \frac{4}{\gamma \Delta g T_p^2} \tag{2.16}$$

If the number of $q$-space points measured is $N_q = \frac{q_{max}}{\Delta q}$, then the sensitivity of our propagator is

$$\frac{v}{\text{pixel}} = \frac{v_{max}}{N_q} \tag{2.17}$$

# Chapter 3

# Experiment

The overarching goal of this experiment was to develop a pulse sequence that rapidly, and effectively measures a bulk flow propagator. There are previous works that employ methods discussed here in order to measure propagators [7], however, in this project, we aim to make these measurements rapidly and more efficiently. To do this, we used a value of $T_R$ equal to that of $T_p$, meaning that we do not allow time for our magnetization to fully recover before applying another RF pulse to excite the sample. In order to do this, we must use small tip angles ($\alpha < 90^o$) so that there is remaining longitudinal magnetization.

## 3.1 Flow Network

This experiment was done by flowing water through the UNB MRI Centre's 2.4 tesla magnet. To do this, we required a reliable flow network that would allow us to flow water at various speeds through a pipe in the bore of the magnet. We could measure the propagator of this flowing water sample. Tap water was chosen as our sample since it gives a strong NMR sample.

Our flow network consisted of a large reservoir filled with water, which fed into a Berkeley BPDH10-L Corrosion-Resistant Self-Priming Sprinkler Pump. A diagram of this network can be seen in Figure (3.1). This pump then pumped water upwards. Above the pump was a junction where water was faced with 2 routes: return to the reservoir or continue flowing up. Each of the 2 pipes had a valve that would allow us to control how much water went which way and therefore the velocity of water in the magnet. In practice, the valve that led to the magnet was either fully open, allowing flow through the magnet, or closed, allowing water to sit stationary in the magnet. The other valve, leading to the reservoir, was to control the speed of the water, as by closing it we could minimize the amount of water recycling to the reservoir, and thus increase the bulk flow rate (and therefore speed) in the magnet. In practice, closing the return valve caused a minimal change in the bulk flow rate from the pump (roughly 0.004 L/s) so 2 flow rates were used: 0 L/s and $0.16 \pm 0.02$ L/s. This non-zero flow rate was measured via a bucket-and-stopwatch technique.

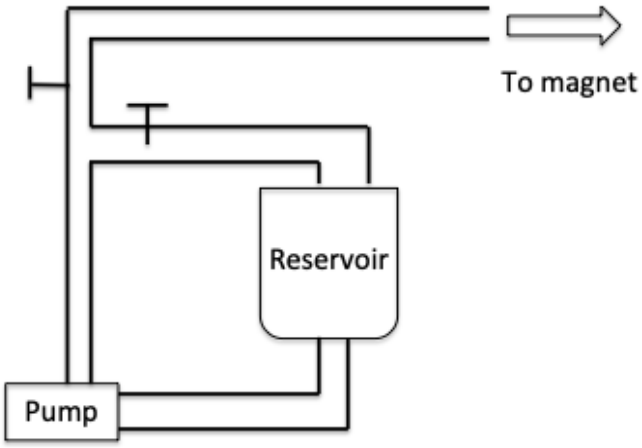


Figure 3.1: A diagram of the flow network used in this experiment

The pipe that was placed in the magnet had two main sections to it: a normal, straight pipe and a constriction. The horizontal cross section of this pipe can be seen in Figure (3.2). This pipe was long enough that we could place either the straight portion or the constriction in the sensitive part of the magnet, allowing us to study the flow in either. The pipe itself had a radius of 1.9 cm which corresponded to an average velocity of $0.561 \pm 0.002$ m/s. The radius of the constriction was a third of that and gave a velocity of $5.049 \pm 0.015$ m/s.

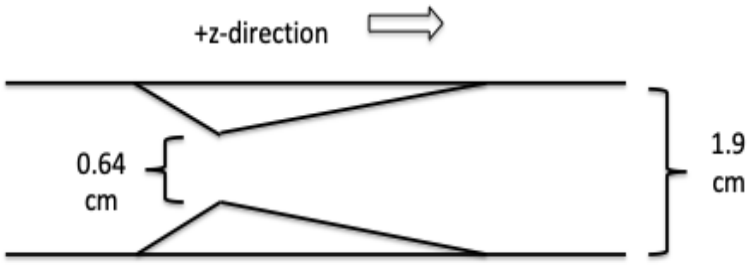


Figure 3.2: A diagram of the pipe in which flow was studied

## 3.2 Pulse Sequences

There were 2 pulse sequences used in this experiment. The first is the one that was discussed in the previous section, and is displayed in Figure (2.3). It begins by acquiring the largest $q$-space point and incrementing its way down through 0 to the smallest $q$-space point. This sequence is certainly the easiest, but may not necessarily acquire the best propagator. With each gradient switch, the current in the gradient coils is reversed. This sudden current switch creates a Lorentz force which mechanically vibrates the magnet. The inductance of the gradient coil windings also prevents the gradient amplifiers from switching the magnetic field gradients perfectly as demanded. For these

reasons, there is motivation to search for a pulse sequence that minimizes the number of gradient switches. One proposed way to do this is to acquire a positive $q$-space point followed by its negative, and repeating this down to 0. A diagram of the pulse sequence that would do this is seen in Figure (3.3).

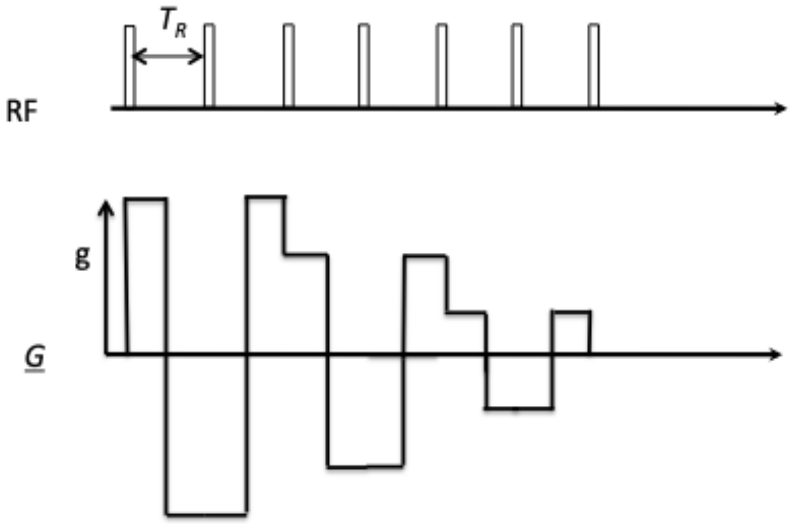


Figure 3.3: An example of a rearranged pulse sequence that measures a bulk flow propagator

In the pulse sequences used in this experiment 32 total $q$-space points were acquired, 16 positive and the corresponding negative 16. This means that our gradient values were incremented by $\Delta g = \frac{g_{max}}{16}$. The maximum gradient value and $T_p$ were varied from experiment to experiment in order to find the parameters that best suited our flow rate and gave us the required sensitivity.

### 3.2.1 Amplitude Trimming

It was mentioned before that switching our gradients quickly cannot be done perfectly. As it turns out, this creates issues (undesired signal attenuation) in the measurement of bulk flow propagators which must be remedied in order to make a successful measurement. There are many methods that can be used in order to ensure that $\int_0^{T_p} g(t)dt = 0$. The one used in this experiment was amplitude trimming. The main issue with this imperfect gradient switch is that one tells the system to achieve a certain gradient value and in reality, it achieves a different value (one lower in magnitude than desired), which leads to an antisymmetric gradient around $\frac{T_p}{2}$. The amplitude trimming solution to this is to tell your system to attempt to achieve a gradient higher than that which is desired, and if the right value is requested from the system, it will reach a value that symmetrizes your gradient by the time $T_p$. Different values of amplitude trimming for each experiment, as $g_{max}$ and $T_p$ were varied, were required.

## 3.3 Acquisition

Data were acquired by implementing the discussed pulse sequences on the aforementioned 2.4 tesla magnet. Maximum motion encoding gradient values ranging from 60% to 100% of the system's maximum possible gradient were used, and the value of $T_p$ was ranged from 400 $\mu s$ to 1 ms. The maximum possible gradient was measured via oscilloscope to be $40 \times 10^{-3}$ T/m. The

gradient values used in the pulse sequence contained values of 1% to 16% (before amplitude trimming) so the actual applied gradient values ranged from $1\% - 16\%$ of $g_{max}$ which ranged from $24 \times 10^{-3}$ T/m - $40 \times 10^{-3}$ T/m.

Stationary and flowing measurements were made in the straight pipe for comparison by completing 32 scans of the bulk propagator pulse sequence. As was mentioned flowing measurements corresponded to 0.56 m/s in this part of the pipe. In the constriction 64 scans were done in order to improve signal-to-noise as there was less water and less coherent flow. These constriction measurements were also done for stationary and flowing samples in order to make comparisons.

# Chapter 4

# Results

In this chapter, we present the results from these experiments. A big part of analysing these data was proving that we did in fact measure the propagators that we meant to measure. A good way to do this is to show that it gives us the same modal velocities that were measured via the bucket-and-stopwatch technique.

## 4.1 Propagators

Of all of the values for $g$ and $T_p$, some yield propagators with a small enough range of flows that we are able to distinguish 0.56 m/s from stationary flow, and some do not. For laminar flow, the propagator is a step function that drops at the maximum velocity [8]. The flow in the pipe yields a Reynolds number of around 8000 however, so there is some turbulence. This turbu-

lence causes the flow to be more sharply peaked. While this peak becomes sharper, it will always have a finite breadth, as it is sensitive to any underlying diffusion occuring in our sample. The propagator of a flowing sample is not centred at zero, and thus if the range of velocities is small enough it appears shifted in comparison with the stationary flow. There are also other differences that correspond to higher moments of the propagator which can be determined from examining a range of $q$-space points that extend farther from the origin.

The figures in this section are of propagators measured using the pulse sequence of Figure (2.3). Figure (4.1) shows a propagator measured with $g_{max} = 60\% = 24 \times 10^{-3}$ T/m and $T_p = 400\ \mu s$. A sensitivity calculation such as that found in Chapter 2 yields $v_{max} = 62.3$ m/s and a sensitivity of $\frac{v}{\text{pixel}} = 3.9$ m/s. This means that our flow of 0.56 m/s should be shifted by roughly 0.15 pixels. This is surely an unnoticeable amount, and we can not see a shifted peak.

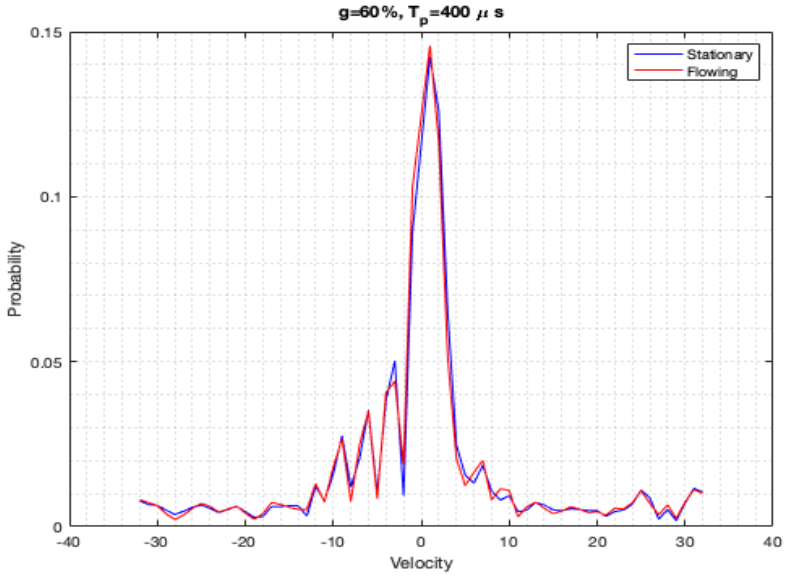


Figure 4.1: A propagator measured with $g = 60\%$ and $T_p = 400\ \mu s$

We can make a small variation on this propagator by changing gradient strength, $g_{max} = 70\% = 28 \times 10^{-3}$ T/m and keeping $T_p$ the same. This gives us a sensitivity of $\frac{v}{\text{pixel}} = 3.3$ m/s, very similar to the previous sensitivity. Again, we see in Figure (4.2) that, as expected, the peak of the propagator is not shifted a discernible amount and we are not sensitive to $v = 0.56$ m/s. There are more oscillations in this propagator, which are likely due to noise.

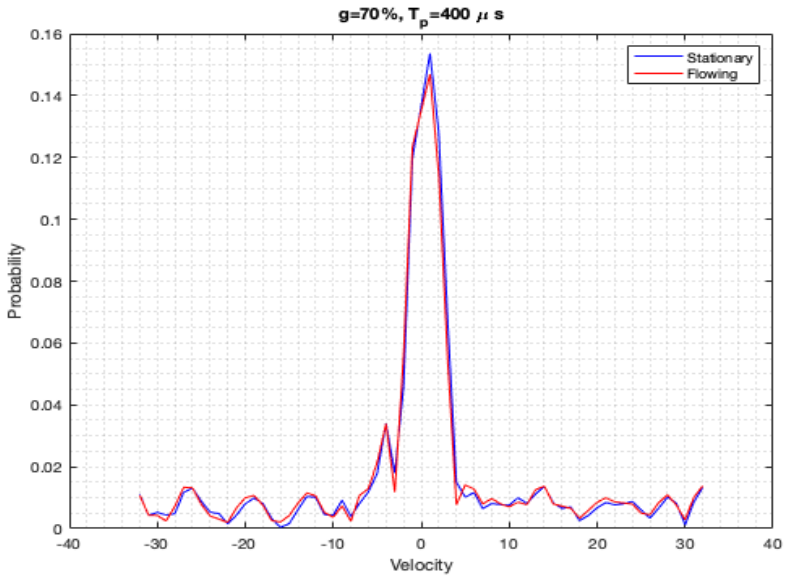


Figure 4.2: A propagator measured with $g = 70\%$ and $T_p = 400\ \mu s$

We can now examine a propagator with better chosen parameters. Figure 4.3 shows a propagator measured with $g_{max} = 70\% = 28 \times 10^{-3}$ T/m and $T_p = 1$ ms. This is improved from the previous two as it has a $T_p$ over twice as large, and as can be seen in equation (2.16), $v_{max} \propto \frac{1}{T_p^2}$. With these parameters, one finds a sensitivity of $\frac{v}{\text{pixel}} = 0.5$ m/s. With this, we expect that our propagator will be shifted by around one pixel. We can see in the figure that we see the expected shift.

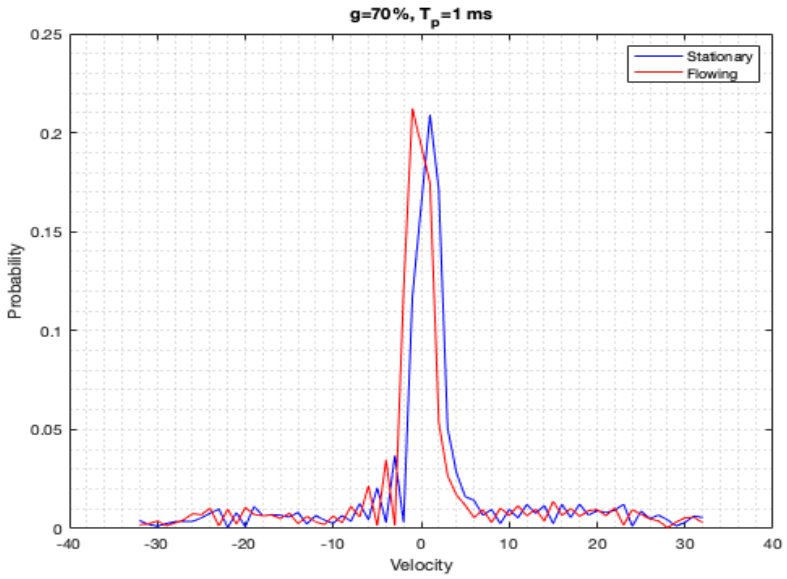


Figure 4.3: A propagator measured with $g = 70\%$ and $T_p = 1$ ms

A variation can be made on this propagator as well, as we can change the maximum gradient to $g_{max} = 80\% = 32 \times 10^{-3}$ T/m and $T_p = 1$ ms still. With these parameters, we find a sensitivity of $\frac{v}{\text{pixel}} = 0.5$ m/s again. This is similar to the last propagator shown, and we should again expect to see a shift of around one pixel. In Figure (4.4) we do in fact see this shift.

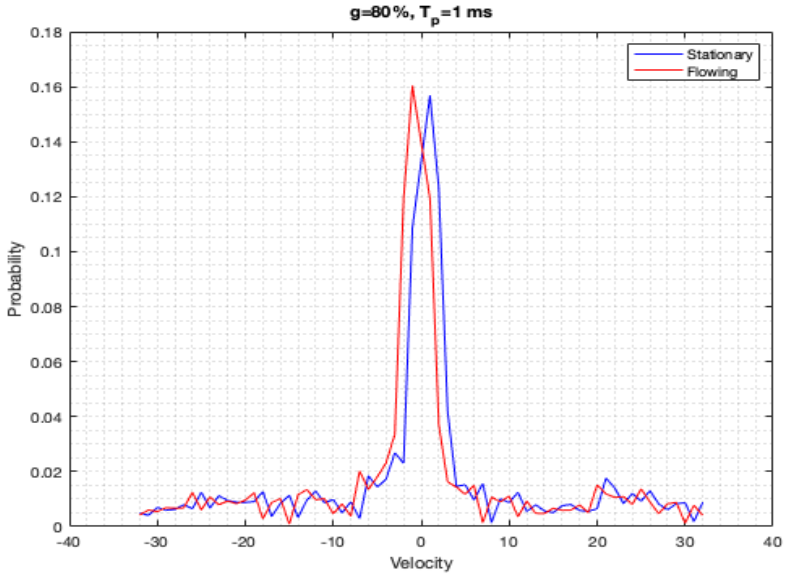


Figure 4.4: A propagator measured with $g = 80\%$ and $T_p = 1$ ms in constriction

So far, all of these propagators have been shown for water flowing through the straight pipe. We can now look at the propagators in the constriction, knowing some good parameters to use. This can be seen in Figure (4.5), with a maximum gradient value of $g_{max} = 80\% = 32 \times 10^{-3}$ T/m and $T_p = 1$ ms. This displays an interesting shape, as we are looking at a wider range of modal velocities. We see in this propagator, features caused by faster flow, and features caused by slower flow, all of which we would expect through this constriction.

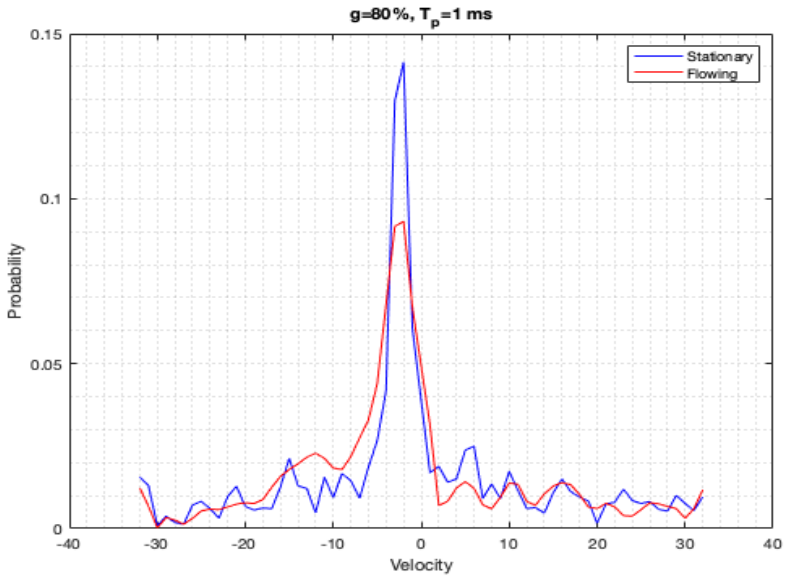


Figure 4.5: A propagator measured with $g = 80\%$ and $T_p = 1$ ms

## 4.2 Corrected Phase

A way to get average velocity information from an NMR signal is by examining the phase. As was seen in Chapter 2, the phase that is accumulated for isochromats as they move in a bipolar magnetic field gradient is

$$\phi = \gamma v \int_0^{T_p} g(t) t dt \tag{4.1}$$

For our bipolar gradients, this evaluates to

$$\phi = -\gamma v g \frac{T_p^2}{4} \tag{4.2}$$

We can thus use this phase to directly calculate the velocity of our flow. To do this, we first correct the phase of our flowing data. There is some instrument dependent phase in the stationary data, so in order to consider phase strictly due to flow, we must rotate our flowing data into the basis defined by the stationary phase, $\phi_s$. This is done by simply multiplying our stationary data by the usual rotation matrix, $R(\phi_s)$.

Once we have these corrected phases, we can use equation (4.2) to measure an average velocity. The phases near $q = 0$ are linear, and their slope against gradient can be measured. Manipulating equation (4.2) and considering changes in phase and gradient, we obtain

$$\frac{\Delta\phi}{\Delta g} = -\frac{\gamma T_p^2}{4} v \tag{4.3}$$

From this, we can obtain the velocity

$$v = -\frac{4}{\gamma T_p^2}\frac{\Delta\phi}{\Delta g} \tag{4.4}$$

The figures below show the corrected phase for the flowing samples discussed above plotted against $g$. Plotted with the phases are the fits that were determined with MatLab's polyfit function, it is the slopes of these fits that were used as $\frac{\Delta\phi}{\Delta g}$.

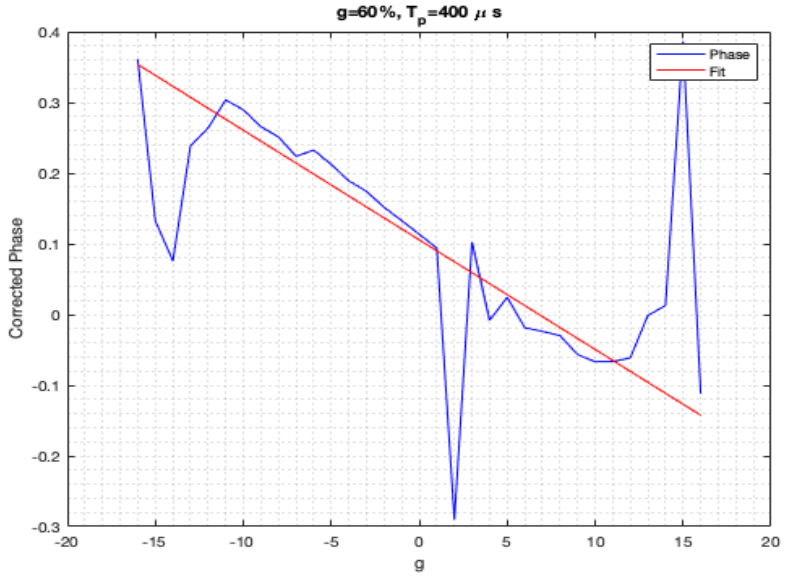


Figure 4.6: Corrected phases measured with $g = 60\%$ and $T_p = 400\ \mu s$

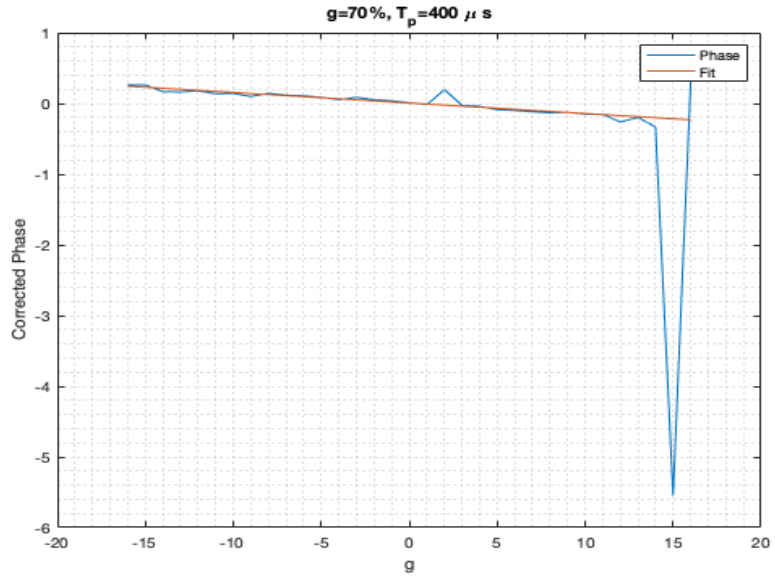


Figure 4.7: Corrected phases measured with $g = 70\%$ and $T_p = 400\ \mu s$

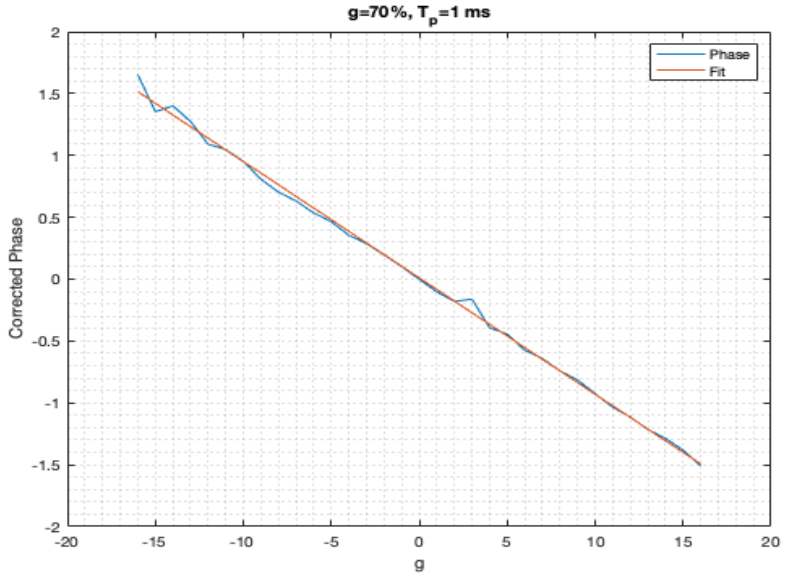


Figure 4.8: Corrected phases measured with $g = 70\%$ and $T_p = 1$ ms

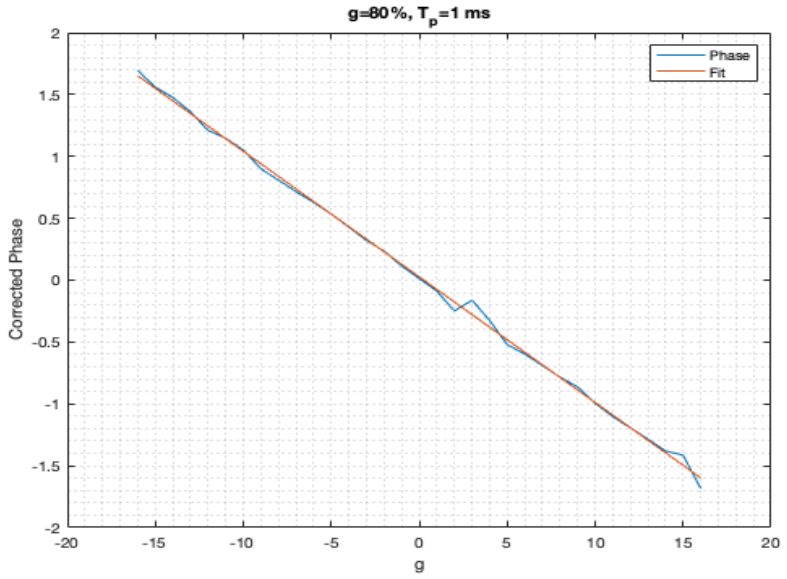


Figure 4.9: Corrected phases measured with $g = 80\%$ and $T_p = 1$ ms

Some of these plots have severe outliers, which were not included in our fit to determine velocity. In Figure (4.6) the first 4 and last 4 points were rejected for our fit, in Figure (4.7) the last 3 points were rejected, and all points from Figure (4.8) and Figure (4.9) were used. From the complete set of measurements, 6 gave slopes which could be used to get a measurement for velocity. These velocities were: 0.43 m/s, 0.85 m/s, 0.80 m/s, 0.7 m/s, 0.75 m/s, 0.69 m/s. These can be averaged to give $\bar{v} = 0.7 \pm 0.15$ m/s. The error on this overlaps with the bucket-and-stopwatch measurement of $0.561 \pm 0.015$ m/s.

Phases can also be measured from the NMR signal in the constriction. Following the same procedure as above, we find the following corrected phases

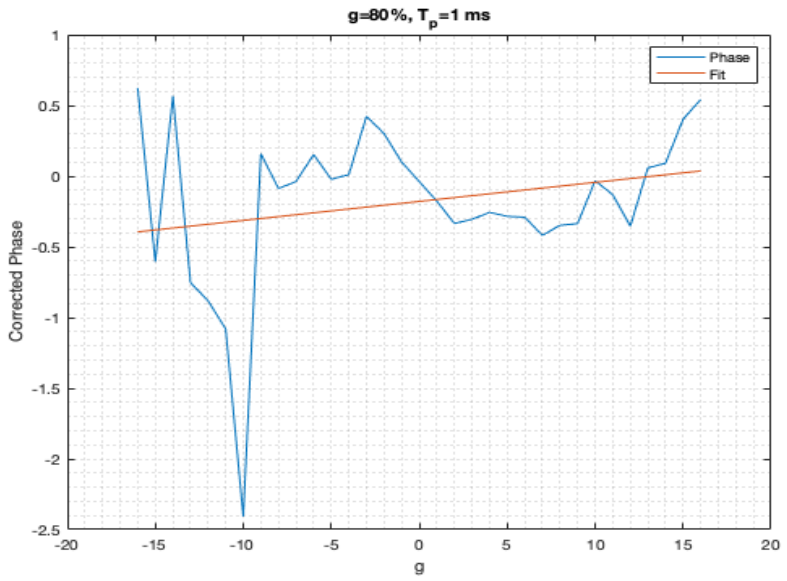


Figure 4.10: Corrected phases measured with $g = 80\%$ and $T_p = 1$ ms in constriction

We can see that these phases do not follow a linear trend that is amenable to a fit, and therefore an average velocity cannot be extracted. This is likely due to a low signal-to-noise, as the flow is channelled through the constriction, as well as an extreme mixing of isochromats, all of which have different histories in this flow, and therefore different phases

## 4.3 Gradient Rearrange

Another part of this project was to find a more effective way of sampling $q$-space in order to measure a bulk flow propagator. A gradient sequence of the form of Figure (3.3) was applied to do this, with the same parameters as the previous propagators. As can be seen below, the propagator was measured with $g_{max} = 80\% = 32 \times 10^{-3}$ T/m and $T_p = 1$ ms. In this we do not exactly see the identical shift, however there is some widening and a slight shift in this propagator.

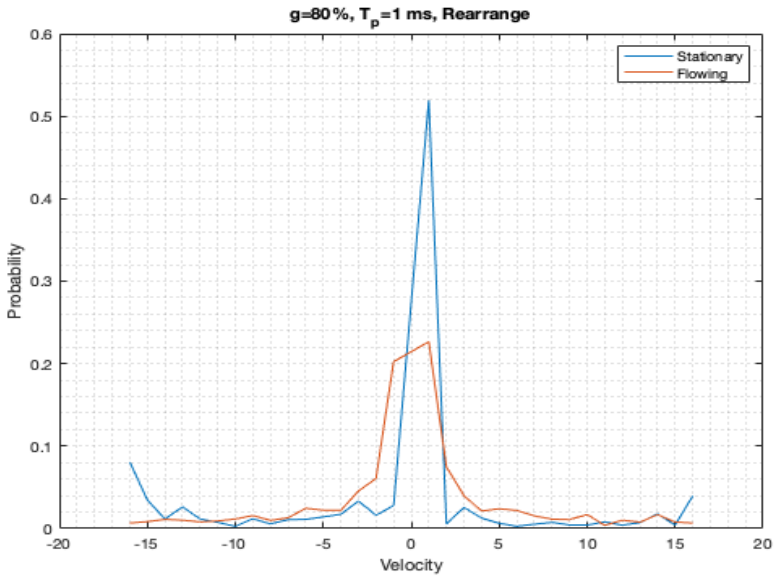


Figure 4.11: A propagator measured with $g = 80\%$ and $T_p = 1$ ms

We can examine the corrected phases for this propagator in a similar manner as before. We see that the positive $q$-space points seem to have a different form than the negative points. This could be due to phase wrapping and issues with rearranging the gradient. The slope of these phases give a velocity of $v = 0.71$ m/s, which is comparable to that with our previous gradient arranging.

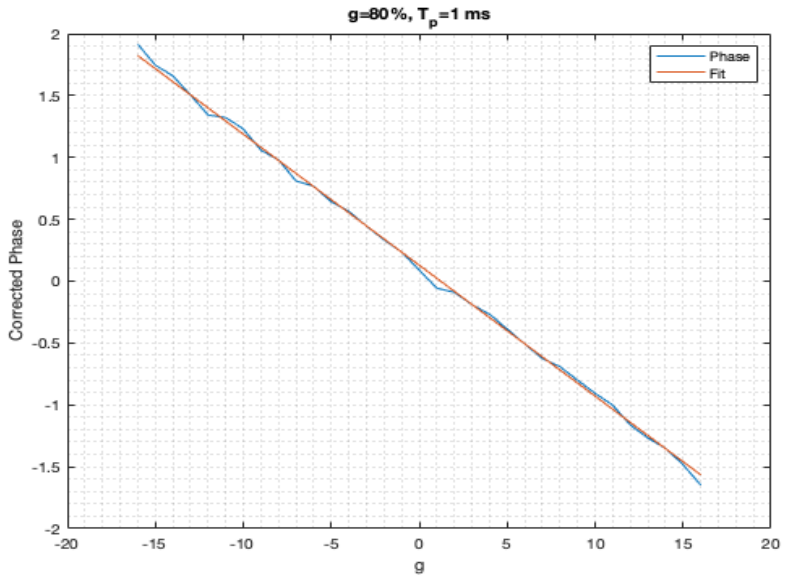


Figure 4.12: Corrected phases measured with $g = 80\%$ and $T_p = 1$ ms

Overall, this method certainly is possible, but more work and fine tuning is required in order to build the confidence in it that we have in the previous gradient arrangement. This should be the primary focus of future work on the rapid measurement of bulk flow propagators.

# Chapter 5

# Conclusion & Future Work

This project yielded interesting results and is in a good place to be expanded on. This project was successful in measuring the intended propagators and we were able to make measurements of the average velocity of a flowing sample. These propagators also have more information of the flow in their higher order moments, which will require a higher signal to noise to measure.

The main next step in this project is to work on rearranging the gradients in order to begin acquiring these propagators with fewer gradient switches, as was mentioned before. With fewer gradient switches, there should be reduced eddy currents which should improve accuracy. This process was started in this project, but not completed, and so this should be the next step.

Overall, as this project set out to develop a pulse sequence to rapidly measure bulk flow propagators, it was successful in doing so, as the standard acquisition time was around two minutes. The results of this project have

also set up future work nicely, as there is certainly more work to be done.

# Bibliography

[1] Paul T. Callaghan. *Principles of Nuclear Magnetic Resonance Microscopy*. Oxford Scientific Publications, 1991.

[2] Jacek W. Kennel, Jacek Klinowski. *Fundamentals of Nuclear Magnetic Resonance*. Longman Scientific and Technical, 1993.

[3] Anatole Abragam. *The Principles of Nuclear Magnetism*. Oxford University Press, 1961.

[4] David J. Griffiths. *Fundamentals of Electrodynamics*. Pearson, fourth edition, 2013.

[5] Paul Callaghan. *Translational Dynamics and Magnetic Resonance: Principles of Pulsed Gradient Spin Echo NMR*. Oxford University Press, 2011.

[6] Paul Callaghan, Yang Xia. Velocity and Diffusion Imaging in Dynamic NMR Microscopy. *Journal of Magnetic Resonance*, 91:326–352, 1991.

[7] Michael L. Johns. Jonathan Mitchell. Rapid Measurements of Diffusion Using PFG: Developments and Applications of the DIFFTRAIN Pulse Sequence. *Concepts in Magnetic Resonance*, 2009.

[8] Benedict Newling. Gas flow measurements by NMR. *Progress in Nuclear Magnetic Resonance Spectroscopy*, 52:31–48, 2008.